

A Correlated Data-Driven Collaborative Beamforming Approach for Energy-efficient IoT Data Transmission

Yangning Li, Hui Kang, Jiahui Li, Geng Sun, *Senior Member, IEEE*, Zemin Sun, Jiacheng Wang, Changyuan Zhao, Dusit Niyato, *Fellow, IEEE*

Abstract—An expansion of Internet of Things (IoTs) has led to significant challenges in wireless data harvesting, dissemination, and energy management due to the massive volumes of data generated by IoT devices. These challenges are exacerbated by data redundancy arising from spatial and temporal correlations. To address these issues, this paper proposes a novel data-driven collaborative beamforming (CB)-based communication framework for IoT networks. Specifically, the framework integrates CB with an overlap-based multi-hop routing protocol (OMRP) to enhance data transmission efficiency while mitigating energy consumption and addressing hot spot issues in remotely deployed IoT networks. Based on the data aggregation to a specific node by OMRP, we formulate a node selection problem for the CB stage, with the objective of optimizing uplink transmission energy consumption. Given the complexity of the problem, we introduce a softmax-based proximal policy optimization with long short-term memory (SoftPPO-LSTM) algorithm to intelligently select CB nodes for improving transmission efficiency. Simulation results validate the effectiveness of the proposed OMRP and SoftPPO-LSTM methods, demonstrating significant improvements over existing routing protocols and node selection strategies. The results also reveal that the combined OMRP with the SoftPPO-LSTM method effectively mitigates hot spot problems and offers superior performance compared to traditional strategies.

Index Terms—Collaborative beamforming, Internet of Things, routing protocols, data fusion, deep reinforcement learning.

I. INTRODUCTION

THE Internet of Things (IoT) has been widely adopted in various monitoring and control applications, such as

This work is supported in part by the National Natural Science Foundation of China (62172186, 62471200, 62272194), in part by the Science and Technology Development Plan Project of Jilin Province (202201011101JC, 20230201087GX, 20240302079GX), and in part by the Postdoctoral Fellowship Program of CPSF (GZC20240592). (*Corresponding authors: Jiahui Li and Geng Sun.*)

Yangning Li, Hui Kang, Jiahui Li, and Zemin Sun are with the College of Computer Science and Technology, Jilin University, Changchun 130012, China, and also with Key Laboratory of Symbolic Computation and Knowledge Engineering of Ministry of Education, Jilin University, Changchun 130012, China (e-mails: ynli23@jlu.edu.cn; kanghui@jlu.edu.cn; lijiahui@jlu.edu.cn, sunzemin@jlu.edu.cn).

Geng Sun is with the College of Computer Science and Technology, Jilin University, Changchun 130012, China, and with Key Laboratory of Symbolic Computation and Knowledge Engineering of Ministry of Education, Jilin University, Changchun 130012, China; he is also affiliated with the College of Computing and Data Science, Nanyang Technological University, Singapore 639798 (e-mail: sungeng@jlu.edu.cn).

Jiacheng Wang, Changyuan Zhao and Dusit Niyato are with the College of Computing and Data Science, Nanyang Technological University, Singapore (e-mails: jiacheng.wang@ntu.edu.sg; zhao0441@e.ntu.edu.sg; dniyato@ntu.edu.sg).

environmental monitoring [1], energy sensing [2], and industrial automation [3]. However, as the scale of IoT networks expands, these IoT devices generate massive data volumes, leading to challenges in wireless data harvesting and dissemination as well as energy management [4]. In particular, there is significant data redundancy among the massive data packets due to spatial and temporal correlations, especially in homogeneous IoT networks [5], [6]. Thus, it is important to manage these vast amounts of data in IoT networks to keep energy efficient and eliminate data redundancy.

Generally, the existing deployment approaches usually place the base station (BS) or sink centrally within the IoT network, and employ the routing protocols to ensure orderly data routing from extensive networks to the BS. However, this scheme may be unsuitable in the remotely deployed IoT networks which are far from the BS or sink. In such cases, the IoT nodes that are closer to the BS often bear a heavier load of relay tasks. Thus, using traditional routing protocols results in excessive energy consumption for the last hop due to geographic distance and data accumulation, which exacerbates hot spot issues [7]. Moreover, the excessive long-distance links also increase the energy consumption of the IoT devices for data transmission.

In this case, collaborative beamforming (CB) can enhance transmission gain for long-distance links between IoT devices and a remote BS. Specifically, multiple IoT devices can form a virtual antenna array (VAA) and synchronize their transmissions, thereby achieving constructive interference at the location of the remote BS. In this case, an ideal CB setup with N collaborating nodes can achieve an N^2 fold increase in power received at the destination. Conversely, for a given threshold of received power, the required transmit power can be decreased by a factor of $1/N^2$ [8]. Thus, CB can compensate for the insufficient transmission gains of IoT devices. Meanwhile, the sufficient transmission gain allows the selection of collaborating nodes to be independent of their geographic distribution, which can significantly mitigate the hot spot issue.

However, existing research on CB in IoT networks has not fully integrated the characteristics of the IoT networks. Specifically, most studies focus on optimizing beam patterns to improve transmission performance (e.g., [9], [10], [11], [12]), while some also address the network lifetime through multi-slot CB optimization (e.g., [13], [14], [15], [16]). Nevertheless, few studies consider the data characteristics and routing challenges within IoT networks. For instance, in some

homogeneous CB-based IoT systems, there is data redundancy among devices, which should ideally be eliminated before uploading the data to the BS. Besides, expecting each node to use CB after data is generated to communicate with a remote BS is impractical due to the potential for collisions and interference. Thus, managing the efficient and organized upload of data is crucial. Furthermore, the optimization of CB should account for the long-term data and energy management of the IoT network, which has received little attention.

Accordingly, we propose a novel, data-driven CB-based approach for data harvesting and dissemination. This approach reduces energy consumption in data transmission by controlling the routing of data sharing among IoT nodes and selecting CB nodes for uplink communication over a timeline. We summarize the key novelty and main contributions of this paper as follows.

- *CB-based Data-driven Long-term Data Harvesting and Dissemination System for IoT*: We introduce CB into a data-driven system for long-term data harvesting and dissemination in IoT networks. In this system, the IoT network aggregates data through routing, eliminates redundancy via data fusion during routing, and then forms a VAA to upload the data to the remote BS. This process is repeated until the IoT nodes deplete their energy. The system is designed from a data-driven perspective, considering the data generation, fusion, and output to the BS. To the best of our knowledge, this is the first exploration of CB-based IoT optimization from a data-driven perspective.
- *Energy-efficient Routing Protocol Based on Data Redundancy Estimation*: We propose an overlap-based multi-hop routing protocol (OMRP) as the routing strategy for the system. Specifically, OMRP adjusts cluster head selection, fusion order, and relay strategy based on data redundancy estimation, thereby optimizing the data aggregation process of the network. As such, a single execution of OMRP aggregates the data from the entire IoT network to a designated node, thereby enhancing energy efficiency and reducing redundancy.
- *DRL-based Node Selection Method Adapted to OMRP*: Proximal Policy Optimization with Long Short-Term Memory (SoftPPO-LSTM) method is used to optimize node selection in the CB stage. After the OMRP routing protocol is executed, the SoftPPO-LSTM method intelligently selects CB nodes to form a VAA. Following the synchronization of data and strategies among CB nodes, the network data is uploaded to the remote BS using CB, ensuring efficient and coordinated transmission.
- *Simulation and Performance Evaluation*: Extensive simulation results demonstrate that the proposed OMRP significantly outperforms various existing routing methods. Additionally, the SoftPPO-LSTM method for node selection surpasses other DRL methods. Furthermore, the combined OMRP with the SoftPPO-LSTM method effectively mitigates the hot spot problem, offering superior performance compared to traditional strategies, such as those based on distance or energy.

The rest of this article is organized as follows. Section II reviews the previous work on routing protocols and CB. Section III introduces the system models. Section IV presents the formulation and analysis. Section V presents the proposed OMRP. Section VI presents the proposed SoftPPO-LSTM node selection method. Section VII gives the simulations and we conclude this paper in Section VIII.

II. RELATED WORKS

In this work, we aim to establish a data-driven, long-term, and energy-efficient communication scheme between IoT and the remote BS through the use of CB and routing protocols. However, these approaches and factors are often considered separately in the literature. To illustrate the novelty of our work, we briefly review some key existing studies.

A. Hierarchical Routing in IoT

In IoT, hierarchical routing is an effective network management strategy for handling data transmission issues in complex networks consisting of a large number of nodes. There are several strategies to enhance the efficiency and performance of hierarchical routing protocols. Firstly, some studies improved the performance of IoT by considering cluster strategy. Heinzelman *et al.* [17] first introduced the concept of clustering and cluster head (CH) selection, the proposed LEACH protocol randomly selected CHs in a round-robin approach and balanced the network energy consumption through IoT nodes taking turns being CHs. Behera *et al.* [18] proposed the R-LEACH protocol, which considered the energy level of nodes and the number of CHs in the CH selection process, and reduced broadcast energy consumption by using the headset mechanism. Secondly, some studies considered multi-hop transmission, which reduces the transmission power of a single node by reducing the communication distance for each node, thereby reducing energy consumption and extending the service life of the node. Chen *et al.* [19] introduced D2CRP, leveraging two-hop neighbor information for cluster formation to enhance energy efficiency. Lin *et al.* [20] proposed CMSTR, a multi-chain routing scheme, which studied the shortest Hamiltonian path problem to establish intra-cluster routing and adopted the multi-hop mode to establish inter-cluster routing. Thirdly, research on data within IoT hierarchical routing often centered on perception maintenance and eliminating redundancy. Wang *et al.* [21] studied the energy-redundantly covered metric on CH selection for the cluster-based routing protocols, and attempted to simulate the most efficient area coverage tessellation, network coverage lifetime to improve network coverage lifespan. Tao *et al.* [22] and Song *et al.* [23] studied the coverage overlap factor to improve both power efficiency and coverage preservation. However, existing work had not considered routing protocols from the perspective of spatial data redundancy.

B. Data-Driven and Data Fusion in IoT

In IoT, data-driven is a core methodology that focuses on leveraging large amounts of data collected from numerous IoT

nodes to guide decision-making and optimize operations[24]. For example, Snigdha *et al.* [25] proposed a multiple-tree architecture to enhance energy efficiency and extend the lifespan by optimizing query-driven data transmissions. Biswas *et al.* [26] developed an event-driven, fault-tolerant routing algorithm, addressing real event detection and erroneous measurements through distributed event detection and multi-objective routing optimization, enhancing both the efficiency and accuracy of data transmission. Jan *et al.* [5] proposed a data-driven aggregation mechanism that effectively addresses spatial correlations in resource-constrained networks, reducing data redundancy and enhancing accuracy through a dual-layer processing architecture at the node and cluster head levels.

Data fusion technology refers to the process of integrating multiple sets of data originating from different sources in order to produce more consistent, accurate, and useful information [6]. For example, Saeidi *et al.* [27] employed the Dempster-Shafer theory to fuse airborne LiDAR data with multispectral imagery, enhancing land cover feature extraction. Their work demonstrated the efficiency and accuracy of the methodology in integrating multi-sensor data without prior knowledge. Wang *et al.* [28] introduced a data fusion algorithm based on hesitant fuzzy entropy, leveraging hesitant fuzzy entropy to enhance decision accuracy by effectively reducing data redundancy and optimizing energy consumption. This approach improved the quality of fused data, ensuring robust and efficient network performance. Yu *et al.* [29] developed a clustering-based data fusion algorithm that incorporated fuzzy logic to enhance data accuracy and reduce redundancy. Their method optimized network energy consumption and extended network lifetime by efficiently clustering nodes using a butterfly-optimized fuzzy algorithm and selectively fusing data through a fuzzy logic controller.

In our study, spatial correlation is considered in the homogeneous IoT network, meaning that nodes closer to each other tend to gather more redundant data. Data fusion technology is used in the routing process to eliminate the redundancy. Moreover, the data collection and harvesting are driven by queries from the BS. The detailed description of the modeling process is provided in Section III.

C. CB in IoT for Energy and Performance

Some existing work considers the use of CB in IoT. For example, Haro *et al.* [30] designed a virtual beamformer via convex optimization, offering both centralized and distributed solutions to extend network lifetime and meet the quality of service requirements by using a random energy consumption model. Sun *et al.* [14] mitigated the maximum sidelobe level by employing hybrid discrete and continuous optimization strategies, alongside both centralized and distributed methodologies, thereby improving transmission range and energy efficiency. Furthermore, Sun *et al.* [9] developed a multi-objective optimization framework for mobile networks, effectively optimizing the maximum side-lobe level, transmission power, and motion energy consumption for distributed CB, achieving enhanced transmission distance and energy efficiency with minimized motion energy expenditure. Bao *et al.* [13] introduced a software-defined energy harvesting architecture

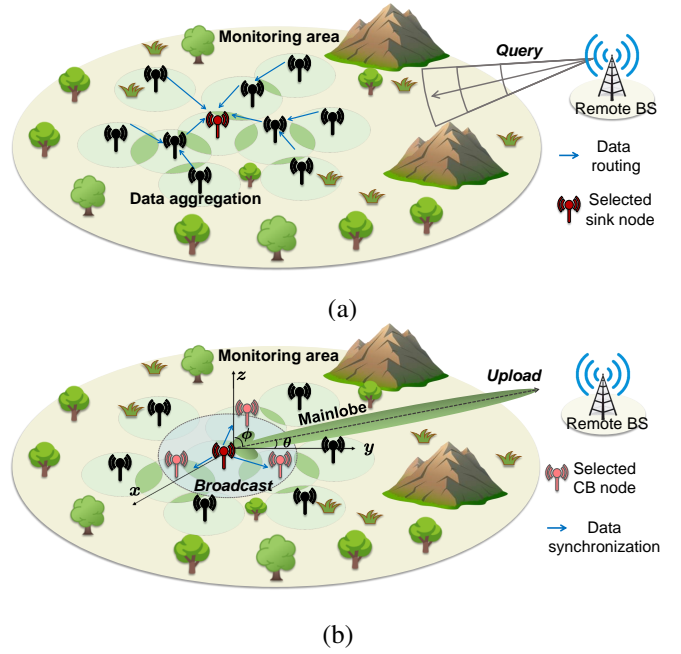


Fig. 1. The CB-based data harvesting and dissemination system overview. (a) The routing process is activated by a query from the BS. (b) Sketch map and geometrical configuration of CB process after aggregating the data to the sink node.

for CB communications, leveraging a reinforcement learning algorithm to optimize beamforming performance while ensuring long-term operation and energy efficiency. However, none of the existing approaches consider the long-term CB optimization with data routing in IoT. Data packets sent during the CB process typically originate from a limited number of IoT nodes. There may be interference and collisions in the CB process without data aggregation, particularly in large IoT networks with a limited number of base stations.

Different from the existing works, our research is different and more significant by considering an integration of routing strategies and the CB method to complete communication processes and long-term network optimization. Specifically, we address the entire sequence of events from the initial data generation by IoT nodes to its eventual upload to the remote BS, with a focus on a data-driven approach throughout.

III. SYSTEM MODEL

In this section, we first present the overview of the considered data-driven IoT data harvesting and dissemination system. Then, we present the system models, including the CB-based communication model, energy consumption model, and data correlation and fusion model. Note that a comprehensive list of the main mathematical notations used in this paper is shown in Table I.

A. System Overview

As is shown in Fig. 1, a CB-based data harvesting and dissemination system for serving a vast homogeneous IoT cluster is considered, in which the monitor area contains massive IoT nodes, the set of which is denoted as $\mathcal{N} = \{1, 2, \dots, N_{IoT}\}$.

Each node has its own monitoring area, and there may be overlapping areas between nodes. We denote the monitoring area of node i with a radius of r as A_i . The neighbor list of node i is the node whose monitoring areas overlap with node i , and their set is defined as $\mathcal{F}_i = \{j | d_{i,j} < 2r, j \in \mathcal{N}\}$, where $d_{i,j}$ is the Euclidean distance of node i and node j . Due to the insufficient transmit power of the IoT nodes and complex terrestrial network environments, it is difficult for a single node to transmit data to a remote BS directly. Therefore, these IoT nodes will gather the data packets through routing policy and communicate with the remote BS by performing CB. We consider that each IoT node is equipped with a single omnidirectional antenna, and the precise location of the IoT node can be obtained through positioning systems or innate settings.

As such, in a certain mission round, the data sensed by the IoT nodes needs to be aggregated and transmitted to the remote BS for the purposes of data backup and perception maintenance. Due to the long-range transmission distance between the IoT cluster and the BS, the minimum receive power threshold at the remote BS is difficult to meet by the transmit power of a single IoT node. Alternately, multiple IoT nodes are expected to form a VAA and perform CB for uplink data transmission. In this work, we define the sink nodes for intro-cluster data aggregation. Accordingly, all IoT nodes need to first use a certain hierarchical routing protocol to transmit data to the sink node, and then the sink node selects candidate nodes and initiates CB to transmit the data to the remote BS.

Fig. 2 shows the designed operation mechanism for the considered CB-based data harvesting and dissemination system. Based on the above analysis, we divide a mission round into six steps, which are listed as follows:

- *Step 1*: The remote BS broadcasts a message to the network to request the collection of monitor data. The message specifies the sink node of the network for this round.
- *Step 2*: After receiving the message, each IoT node rebroadcasts it in order to search for neighbors.
- *Step 3*: The IoT nodes execute a specific hierarchical routing protocol to determine the network topology and TDMA schedule.
- *Step 4*: The IoT nodes perform data routing and fusion according to the established network topology and TDMA schedule. Note that data fusion is performed at the receiver, and the fused data of the network is finally collected at the sink node.
- *Step 5*: The sink node executes the node selection strategy based on the collected network information, and the selected nodes are regarded as beamforming nodes. The sink node broadcasts data and strategies to the beamforming nodes for CB preparation.
- *Step 6*: The beamforming nodes perform CB and send the fused data to the remote BS.

Without loss of generality, we consider a 3D Cartesian coordinate system, and the positions of the antenna of i th IoT node and the remote BS are represented as $(x_i^{IoT}, y_i^{IoT}, h^{IoT})$ and (x^{BS}, y^{BS}, h^{BS}) , respectively. Subsequently, we detail

the key models with respect to data transmission and fusion including the CB-based communication model, energy model, and data correlation and fusion model.

TABLE I
NOTATIONS OF THE MAIN CONCEPTIONS

	Symbols	Definition
System Model	A_i	The monitoring area of IoT node i
	h^{IoT}, h^{BS}	Altitudes of the IoT nodes and the remote BS
	\mathcal{N}	The set of the IoT nodes
	N_{IoT}, N_{CB}	The total number of IoT nodes and that of nodes performing CB
	$d_{i,j}$	The Euclidean distance between nodes i and j
	\mathcal{F}_i	The neighbor list of node i
	G_r, G_t	Receiving gain at the BS and transmitting gain of CB
	P_r, P_t	Received power at the BS and transmitting power of CB
	M_i, m_{ij}	The fusion sequence of node i and its j th node
	q_0	Energy dissipation-data fusion
	r	The monitoring radius of IoT nodes
	E_{elec}	Energy dissipation-electronic circuit
	$\varepsilon_{fs}, \varepsilon_{mp}$	Energy dissipation of free space and multipath amplifiers
	C_i^j	Data packet size after the fusion with the j th node in M_i
	$\alpha_{i,j}$	The fusion rate between two autonomous nodes i and j
	$\beta_{i,j}$	Distance factor for node i selecting node j as a relay node
	E_0	Initial energy of each IoT node
	ρ_i	Ratio of the overlapping area between node i and its neighbors
	\mathcal{G}_t	The topology of the network in the t th round
	Algorithm	$\mathcal{N}_t, \mathcal{E}_t$
T_i		The survival time of node i
$T_{(i)}$		The i th element in the sorted survival times of the nodes
S, \mathbf{s}		State space and state vector of environment
\mathcal{A}, \mathbf{a}		Action space and action vector of agent
\mathcal{R}, \mathbf{r}		Reward space and reward
\mathcal{P}		State transition probability of environment
γ		Discount factor
$e_i(t)$		The residual energy of node i in the t th round
$v_i(t)$		The score of node i as a beamforming node in the t th round
ζ_1, ζ_2	The weights assigned to the throughput and the energy cost	
$\theta_{Q_{new}}, \theta_{Q_{old}}$	The parameters of the new and old actor networks	
θ_c, θ_f	The parameters of the critic network and the feature network	

B. CB-based Communication Model

In the CB-based communication model, the positions, transmission power, and initial phase of beamforming nodes determine the performance of communication. Specifically, we let (ϕ, θ) denote any direction centered on the VAA, where $\phi \in [0, \pi]$ and $\theta \in [-\pi, \pi]$ are the elevation and azimuth angles, respectively. According to the electromagnetic wave superposition principle, the array factor (AF) of N_{CB} nodes can be approximated as follows [31]:

$$\text{AF}(\phi, \theta, I) = \sum_{k=1}^{N_{CB}} I_k e^{j\Psi_k} e^{j\frac{2\pi}{\lambda} d_k(\phi, \theta)}, \quad (1)$$

where λ is the wavelength, I_k and Ψ_k are the excitation current weight and initial phase of the k th node, respectively. Furthermore, Ψ_k is defined as follows:

$$\Psi_k = -\frac{2\pi}{\lambda} d_k(\phi, \theta), \quad (2)$$

where $d_k(\phi, \theta)$ is the Euclidean metric between the k th IoT node and the target BS, and it is expressed as follows:

$$d_k(\phi, \theta) = \sqrt{L^2 + r_k^2 - 2r_k L \sin(\theta) \cos(\phi - \delta_k)}, \quad (3)$$

where r_k and δ_k collectively define the polar coordinates of the k th node.

Considering the long distance between the sensing area and the remote BS, the two-ray multipath fading model is used, and the received power at the remote BS is given as follows:

$$P_r = \frac{P_t G_t G_r h_t^2 h_r^2}{d^4}, \quad (4)$$

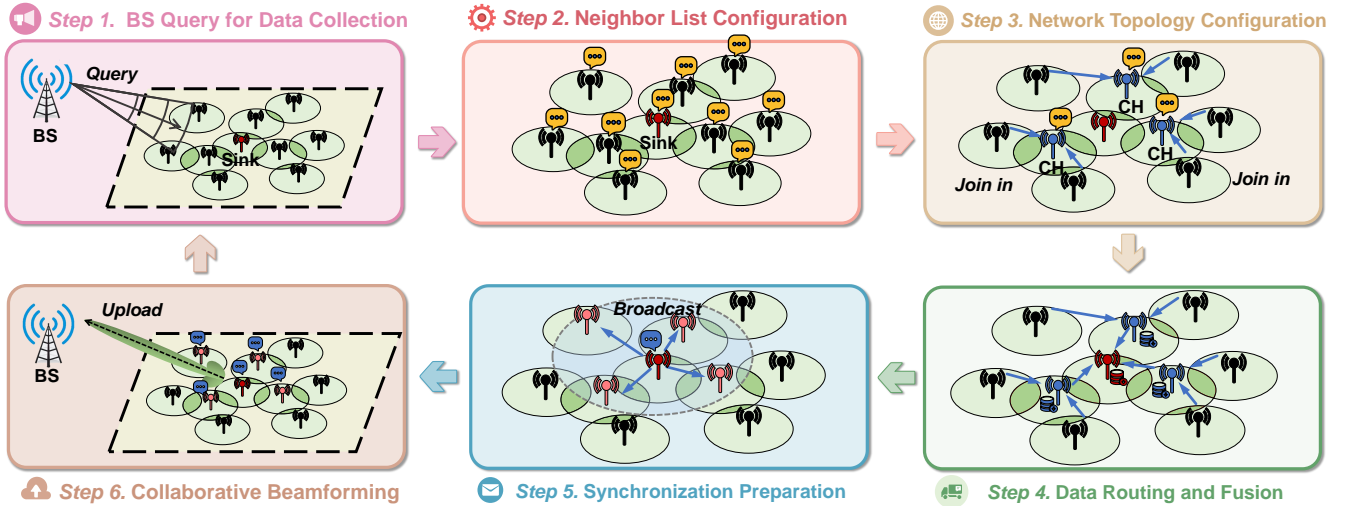


Fig. 2. Network model and operating mechanisms. Each round of data harvesting consists of six steps. Routing and fusion are configured and performed in steps 3 and 4, while synchronization and CB are performed in steps 5 and 6.

where P_t , G_r , and G_t represent total transmitting power, receiving gain of BS, and transmitting gain of CB, respectively. Moreover, h_t and h_r are the heights of the IoT nodes and BS, and d is the distance between BS and the center of collaborating nodes.

Therefore, the transmission rate from beamforming nodes to BS is as follows:

$$R_{BS} = B \log_2 \left(1 + \frac{P_r}{\sigma^2} \right), \quad (5)$$

where B is the bandwidth, and σ^2 is the noise power.

Based on the above analyses, more beamforming nodes and higher excitation current weight lead to higher received power and transmission rate. However, this will result in more energy consumption during the transmission process.

C. Energy Model in the Transmission Process of IoTs

The energy consumption during the transmission process mainly consists of two parts, which are short-distance communication between nodes and long-distance CB communication between the nodes and the BS. Specifically, the typical first-order radio model [32] is used for inter-node communication. Short-distance communication between the nodes considers the free space model and long-distance transmission follows the multipath fading model. The energy required to send and receive b -bit packets over a distance d is given as follows:

$$E_T(b, d) = \begin{cases} b \cdot E_{elec} + b \cdot \varepsilon_{fs} \cdot d^2, & d < d_0 \\ b \cdot E_{elec} + b \cdot \varepsilon_{amp} \cdot d^4, & d \geq d_0 \end{cases}, \quad (6)$$

$$E_R(b) = b \cdot E_{elec}, \quad (7)$$

where E_{elec} denotes the per bit energy dissipation that is used for running the transmitter and receiver electronic circuits. Moreover, ε_{fs} and ε_{amp} represent the energy of amplifier for free-space fading and multipath fading, respectively. Finally, d_0 is the distance threshold to determine the two fading models.

Besides, the total energy consumption of the beamforming nodes during the CB process is as follows:

$$E_{CB} = \sum_{k=1}^{N_{CB}} I_k^2 P_0 \cdot \frac{C}{R_{BS}}, \quad (8)$$

where P_0 is the maximum transmission power with an excitation current of 1, and C is the size of the data packet after data fusion at the sink node and is also the final packet size to be sent in the CB process.

In general, a larger data volume in transmission leads to more energy consumption. Therefore, it is crucial to eliminate redundancy and fuse data efficiently.

D. Data Correlation and Fusion Model of IoTs

In this model, data collected by individual nodes in each round exhibit spatial correlation, and these nodes can eliminate the redundancy through data fusion [33]. Generally, a proximity of two independent nodes leads to a bigger overlapping monitoring area and tends to increase the redundancy of the data they collect. Without loss of generality, we use spatial monitoring areas to define the correlation model. Specifically, the data redundancy rate between two nodes is zero if there is no overlapping monitoring area. On the contrary, as illustrated in Fig. 3, overlapping areas within their sensing ranges become evident. The magnitude of the overlapping area serves as an indicator of the data redundancy of these nodes. In this case, the fusion rate $\alpha_{i,j}$ between two autonomous nodes i and j is defined as follows:

$$\alpha_{i,j} = \frac{1}{A_i} |A_i \cap A_j|. \quad (9)$$

Moreover, the fused data packet can be further fused with another packet, the fusion rate is determined by the spatial distribution represented by the data packets. For example, let $M_i = \langle m_{i0}, m_{i1}, \dots, m_{i|M_i|} \rangle$ denote the fusion sequence of node i , where m_{ij} denotes the j th node in the fusion sequence

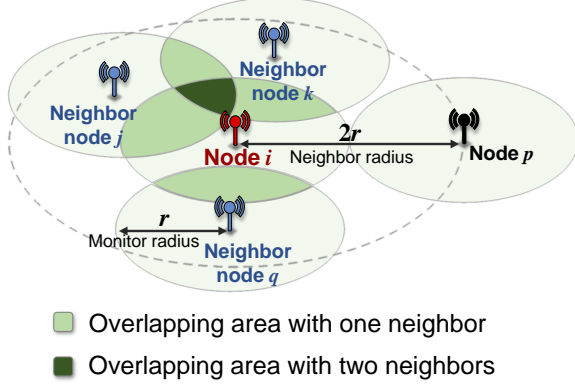


Fig. 3. Overlapping area of node i with its neighbors j , k and q . Note that each node has a monitor radius of r .

for node i , and then the fusion rate between node i and node m_{ij} is as follows:

$$\alpha_{i,j} = \frac{1}{A_{m_{ij}}} \bigcup_{k=0}^{j-1} A_{m_{ik}} \cap A_{m_{ij}}, \quad (10)$$

where $A_{m_{ij}}$ is the monitoring area of node m_{ij} . Following this, the size of the fused data packet at node i in this process changes as follows:

$$C_i^j = C_i^{j-1} + (1 - \alpha_{i,j})|A_j|, \quad (11)$$

where C_i^j represents the size of the data packet after data fusion between node i and the j th node in M_i . Note that the data redundancy eliminated in the data fusion process essentially arises from the overlap of spatial sensing data. In this scenario, regardless of the routing methods used, the size of the data packets collected by the IoT nodes, which have the same spatial distribution, remains constant after efficient data fusion. The fused data will have a smaller data size, thereby saving energy during the next hop transmission process.

In the fusion process, downstream nodes (*i.e.*, the nodes that receive the data packets) can scan two packets separately, eliminate redundancy, and generate the fused packet. In this process, the fusion energy cost is calculated as follows:

$$E_{fusion} = q_0(C_1 + C_2), \quad (12)$$

where q_0 is the standard fusion cost [34], and C_1 and C_2 are the sizes of two packets to be fused, respectively.

IV. PROBLEM DESCRIPTION AND ANALYSIS

In this section, we provide a comprehensive description and analysis of the problem, focusing on the challenges associated with maximizing the network lifetime and total throughput to the remote BS. We describe the roles of nodes, formulate the network topology and node selection mathematically, and introduce our motivation for using routing and beamforming methods to jointly optimize network performance.

A. Problem Description

The main goal of the considered system is to maximize the network transmission efficiency to the remote BS. This efficiency is determined by two key factors, namely network lifetime and throughput. In each round of tasks, the system needs to assign different working roles to nodes based on their residual energy and locations within the network as efficiently as possible.

Nodes in the considered system can perform multiple roles. On the one hand, nodes can function as both senders and receivers of data. Upon receiving data from upstream nodes (*i.e.*, the nodes that send the data packets), these nodes might either forward it directly as relay nodes or send it to the downstream nodes after fusing the data. These varying roles shape the topology of the network and routing process, and influence the energy consumption in data fusion and transmission. On the other hand, nodes may be required to act as beamforming nodes during the CB phase to enhance signal gain and energy efficiency, or just to remain idle to save energy. The assignment of beamforming roles impacts both the quality of communication and the residual energy of the nodes.

B. Problem Analysis

To address these varying roles and their impacts effectively, it is essential to make informed decisions about network topology and node selection at different stages of the network lifetime, as decisions may need to adapt over time to ensure optimal performance.

Mathematically, let a directed graph $\mathcal{G}_t = (\mathcal{N}_t, \mathcal{E}_t)$ denote the topology of the network in the t th round, where \mathcal{N}_t is the set of alive nodes, and $\mathcal{E}_t = \{x_{ji} | x_{ji} \in \{0, 1, 2\}, j \in \mathcal{N}_t, i \in \mathcal{N}_t\}$ is the state set of directed links. In particular, the state variable x_{ji} indicates whether to select node j to send data to node i and perform data fusion, and x_{ji} is defined as follows:

$$x_{ji} = \begin{cases} 0, & j \text{ has no directed links to } i \\ 1, & j \text{ sends forwards data to } i, i \text{ forwards it} \\ 2, & j \in M_i, i \text{ fuses the data and forwards it} \end{cases} \quad (13)$$

where the difference between state $x_{ji} = 2$ and state $x_{ji} = 1$ is whether the node i fuses the data from the upstream node j or not.

In summary, Eqs. (6), (7), (8), (12) and (13) provide the energy consumption of the IoT nodes in the considered system. Specifically, the network topology and role assignment jointly affect the transmission, reception, and fusion energy consumption in the routing phase. In addition, the final packet size and the selection of beamforming nodes affect the transmission and reception energy consumption for data synchronization (See Step 5 of Fig. 2). Finally, the excitation current weight of the beamforming node and the final packet size determine the beamforming energy consumption in the CB process. Considering the six energy consumption components mentioned

above, the normalized total power consumption of node i , denoted as W_i , is calculated as follows:

$$W_i = \frac{1}{E_0} \left[E_T(C_i^{|M_i|}, d_{i,h}) + \sum_{j \in M_i} E_R(C_j^{|M_j|}) + \sum_{j \in M_i} q_0(C_i^{j-1} + C_j^{|M_j|}) + I_i^2 P_0 \cdot \frac{C_s^{|M_s|}}{R_{BS}} + \bar{E}_R(C_s^{|M_s|}) + \bar{E}_T(C_{i=s}^{|M_s|}, d_{i,m}) \right], \quad (14)$$

where s , h and $C_s^{|M_s|}$ denote the sink node, the next hop of node i and the final packet size, respectively. Additionally, E_0 , $\bar{E}_R(C_s^{|M_s|})$ and $\bar{E}_T(C_{i=s}^{|M_s|}, d_{i,m})$ are the amount of initial energy, the average received and broadcast energy consumption when node i acts as a beamforming node or a sink node, respectively.

Based on the above analysis, this problem involves long-term network topology management and role assignment, making it difficult to solve with a single method. In addition, existing studies usually consider routing and CB strategies of IoT networks separately. This motivates the joint design of two methods for solving the routing and collaborative beamforming problems.

Next, we introduce the routing and data fusion method based on OMRP, which manages network topology and aggregates fused data at the sink node. Then, we present the CB method based on SoftPPO-LSTM, which selects beamforming nodes based on node distribution and residual energy. The two methods jointly optimize the network lifetime and total throughput to the remote BS.

V. THE PROPOSED OVERLAP-BASED MULTI-HOP ROUTING PROTOCOL FOR ROUTING AND DATA FUSION

In this section, we introduce the proposed OMRP routing method, which is based on the location and residual energy of nodes. OMRP operates during the third and fourth steps of each round within the system (See Fig. 2). During these steps, OMRP organizes the network into clusters according to the distribution of CHs. These CHs are responsible for gathering and fusing data packets from the cluster nodes before transmitting the data to the sink node via direct or multi-hop communication. The protocol leverages spatial data correlation to direct CH selection, data fusion sequence, and relay schemes within the IoT network. Similar to other classic protocols such as the LEACH protocol and its latest variants [1], [17], [19], OMRP is designed with three stages, which are the set-up stage, the formation stage, and the data routing stage, and we detail them as follows.

A. Set-up Stage

In the set-up stage, the proposed OMRP aims to update the neighbor list \mathcal{F} and overlapping degree ρ of each node, thereby determining the CHs of the network. To this end, each node is configured with an initial neighbor list \mathcal{F}_i when the network is first deployed. Then, if a node approaches energy depletion, this node will broadcast the *SLP_notify* message to

its neighbors, prompting them to update their neighbor lists. Based on the updated neighbor lists, the overlapping degree of these nodes can be determined. Let ρ_i represent the ratio of the overlapping area with its neighbors to the total sensing area of node i . This ratio is given by

$$\rho_i = \frac{1}{A_i} \bigcup_{j \in \mathcal{F}_i} A_i \cap A_j, \quad (15)$$

where A_i and \mathcal{F}_i are the sensing area and neighbor list of node i , and $A_i \cap A_j$ denotes the area node i overlaps with its neighbor j . Fig. 3 illustrates an example of the overlapping area between a node and its three neighbors. Evidently, we have $0 \leq \rho_i \leq 1$, and when $\rho_i = 1$, it means that the sensing area of node i is completely covered by its neighbors.

Furthermore, a node with a higher overlapping degree indicates that its sensing area is more extensively covered by neighboring nodes, resulting in increased redundancy in the sensed data during the fusion process. In other words, nodes with a larger overlapping degree add fewer unique data elements to the final packet set after fusion, due to the higher redundancy in their sensed data. Additionally, since a higher overlapping degree suggests the presence of more neighboring nodes, it is likely located at the center of a cluster, making it a more suitable candidate to be selected as a CH.

Therefore, we introduce the overlapping degree ρ in the CH election process. Similar to the CH election mechanism in the LEACH protocol, we design a threshold function to determine the probability of a node being selected as a CH. This threshold function is defined as follows:

$$T(i) = \begin{cases} \frac{P}{1 - P \times (r \bmod \frac{1}{P})} K^{\rho_i} & i \in G \\ 0, & \text{otherwise} \end{cases}, \quad (16)$$

where P and K are two constants representing the lower bound ratio of CH nodes to all nodes and an amplification factor with a minimum value of 1, respectively. Moreover, r is the number of rounds since the last election of the cluster head, and the elements in the set G are the nodes that have not successfully campaigned for CH nodes in the latest $r \bmod (1/P)$ round.

As such, in the CH election process, each node generates a random number between 0 and 1, determining the CH election result by comparing it with $T(i)$. Specifically, if the random number is less than the threshold value $T(i)$, the node is automatically elected as a CH and notifies other nodes by broadcasting the *CH_notify* message within the network. Note that $1 \leq K^{\rho_i} \leq K$ is satisfied in the Eq. (16), where K^{ρ_i} serves as the amplification factor to increase the likelihood of nodes with larger overlapping degrees being elected as CHs. Based on the above analysis, this approach increases the possibility of nodes with geographical advantages being elected as CHs, thereby improving the network energy efficiency.

B. Network Formation Stage

This stage primarily establishes the communication topology and timing schedule within clusters and between clusters.

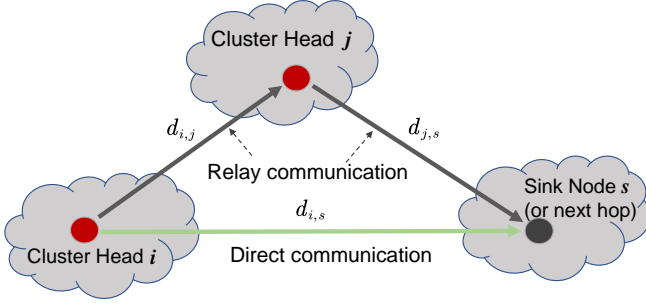


Fig. 4. Direct or relay communication method in inter-cluster routing.

On the one hand, the communication topology and timing schedule within the cluster are determined by the CHs. Specifically, the CHs broadcast CH_notify messages within the network, following which the member nodes assess the signal strength of the broadcast and determine which cluster to join. Then, each member node transmits $JOIN_IN$ message to its CH, following which the CH will extract the overlapping degrees from the received $JOIN_IN$ messages and sort them in descending order. Finally, the CHs calculate and broadcast the TDMA schedule according to this order, allowing member nodes to transmit data in separate time slots to avoid data collision. In this scenario, node data packets with a higher overlapping degree undergo an earlier fusion, leading to more energy savings in the subsequent fusion process due to the reduced fused packet size.

On the other hand, the communication topology and timing schedule between clusters are determined by the communication scheme between CHs and the sink node. Typically, CHs may forward data packets to the sink node via single-hop or multi-hop methods. Although relay communication can significantly reduce transmission energy consumption by reducing the distance, incompletely fused data will cause additional receiving energy consumption according to Eq. (7). Consequently, the selection of the next hop for the CHs in OMRP is based on the specific network cluster distribution.

Accordingly, we will clarify the principles and mechanisms of next-hop selection in OMRP by analyzing a typical scenario shown in Fig. 4. Specifically, CH i has two methods to communicate with the sink node (or next hop), either treating CH j as a relay node or direct communication. Assume that the distance between all nodes is less than the threshold d_0 and the transmission energy dissipation follows the free-space fading model. According to Eqs. (6), (7) and (12), the energy consumption of the relay scheme is given by

$$\underbrace{2bE_{elec}}_{j,s \text{ receive}} + \underbrace{2bE_{elec} + b\varepsilon_{fs} \{d_{i,j}^2 + d_{j,s}^2\}}_{i-j-s \text{ trans}} + bE_{fusion}, \quad (17)$$

where $d_{i,j}$ is the distance between node i and node j . While the energy consumption for direct communication is given by

$$\underbrace{bE_{elec}}_{s \text{ receive}} + \underbrace{bE_{elec} + b\varepsilon_{fs}d_{i,s}^2}_{i \text{ trans}} + bE_{fusion}. \quad (18)$$

Algorithm 1:

Set-up and Network Formation of OMRP

1 Initialization:

Receive query message from the BS calculate ρ_i according to Eq. (15). $CH \leftarrow \emptyset, SN \leftarrow \emptyset$.

2 // Set-up Stage

3 **if** IoT node i runs out of energy **then**

4 | i broadcasts SLP_notify message;

5 **if** IoT node j receives SLP_notify message from neighbor k **then**

6 | Recalculate ρ_j without considering neighbor k according to Eq. (15);

7 **if** i is in G **then**

8 | $T(i) \leftarrow K^{\rho_i} * p / (1 - p(r \bmod 1/p))$;

9 **else**

10 | $T(i) \leftarrow 0$;

11 // Network Formation Stage

12 IoT node i listens to CH_notify message;

13 **if** i 's random number $< T(i)$ **then**

14 | i broadcasts CH_notify message;

15 Remove i from G ;

16 Add i to CH ;

17 **else**

18 Add i to G ;

19 Add i to SN ;

20 **if** $i \in CH$ **then**

21 **for each** $c_j \in CH$ **do**

22 | Add (β_j, c_j) to D_i ;

23 Find β_{max} in D_i and get c_{max} ;

24 **if** $\beta_{max} > 2E_{elec}/\varepsilon_{fs}$ **then**

25 | i sends a $RELAY$ message to c_{max} ;

26 | Form relay agreement between i and c_{max} ;

27 **else if** $i \in SN$ **then**

28 | i joins the closest cluster;

29 Start data transmission;

30 $r \leftarrow r + 1$;

As can be seen, the energy difference between the two methods is defined as Δ , which is given by

$$\Delta = 2bE_{elec} + b\varepsilon_{fs} \{d_{i,j}^2 + d_{j,s}^2 - d_{i,s}^2\}. \quad (19)$$

This difference determines which method is more energy-efficient. To facilitate the choice of an optimal relay node, we define the distance factor for node i selecting node j as a relay node as $\beta_{i,j} = d_{i,s}^2 - \{d_{i,j}^2 + d_{j,s}^2\}$, and the candidate relay node is determined by $\beta_{max} = \max\{\beta_{i,1}, \beta_{i,2}, \dots, \beta_{i,j}\}$. According to Eq. (19), the relay scheme remains more energy-efficient than the direct communication scheme when $\beta_{max} > \frac{2E_{elec}}{\varepsilon_{fs}}$. In this case, the proposed OMRP utilizes the energy-saving relay scheme. The detailed derivation process is shown in Appendix A. We summarize the designed set-up and network formation stages in Algorithm 1.

C. Data Routing Stage

In this stage, each node will act as a sender or receiver at a specific time according to the topology and timing schedule

Algorithm 2:

Intracluster and Intercluster Routing of OMRP

```

1 for  $c_j \in CH$  do
2   Listen JOIN_IN messages from SN;
3   Get  $\mathcal{R} = \{\rho_1, \rho_2, \dots, \rho_m\}$  from
   JOIN_IN messages;
4   Sort  $\mathcal{R}$  in descending order;
5   Broadcast timing schedule according  $\mathcal{R}$ ;
6 if  $i \in SN$  then
7   Transmit data to  $i$ 's CH by schedule;
8 if  $i \in CH$  then
9   while  $time < timing\ schedule$  do
10     $i$  listens and receives data;
11    if  $i$  receives data from cluster member then
12    | Fuse data;
13    Transmit data to next hop using CSMA;

```

determined in the network formation stage, and eventually all the data packets in the network will be collected and forwarded to the sink node. On the one hand, during the allocated time slot for each member node in the cluster, the sensed data is transmitted to its CH while only the transmitting node remains active, and other member nodes in the cluster turn off their transceivers to save energy. Upon receiving a new data packet, the CH performs data fusion and stores the fused data. On the other hand, after collecting all the packets of their cluster or the time exceeds the timing schedule, the CHs employ CSMA for the subsequent hop transmission and forward the packets to the sink node. Finally, the sink node fuses the received packets and generates the final packets of this round. We summarize the data routing stage in Algorithm 2.

After executing OMRP during the third and fourth steps of the system (See Fig. 2), the data packets of the network are gathered and fused at the sink node. The next section will introduce the proposed SoftPPO-LSTM-based CB method, which is designed for data transmission to the remote BS.

VI. THE PROPOSED SOFTPPO-LSTM FOR CB

In this section, we present the proposed SoftPPO-LSTM, which is adapted to the routing method. The SoftPPO-LSTM operates during the fifth and sixth steps of each round within the system (See Fig. 2). Specifically, the sink node collects and aggregates the data, selects enough adjacent nodes as beamforming nodes, synchronizes the data and CB strategy with them, and collaboratively transmits the data to the remote BS using CB. During this stage, the selection and excitation current weights of the nodes need to be optimized. In this paper, we utilize the DRL method to obtain an optimal CB policy. The motivations for using DRL, the node selection problem formulation, the MDP formulation, and our proposed SoftPPO-LSTM algorithm are as follows.

A. Motivations for Using DRL

For the CB scheme, there are several factors, including distance, residual energy, and node location, need to be considered. For example, the nodes far away from the sink node

will cause excessive transmission energy consumption in the data synchronization process. Moreover, the nodes with low residual energy participating in CB may accelerate their energy depletion. In addition, the nodes located at the network edge are typically not near the sink node. Note that the sink nodes of different rounds may change, and the residual energy of the nodes may also decrease at different rates. The dynamic nature of the above factors requires an online method to determine the CB strategy. Similarly, since the considered optimization objective is on a long-term time scale of multiple rounds, the CB strategy needs to balance both the long-term and short-term benefits.

Considering the aforementioned reasons, DRL is a suitable method for CB because it excels at intuitively learning node strategies for different geographic contexts, thereby overcoming the limitations of traditional methods.

B. CB Node Selection Problem Formulation

The DRL algorithm optimizes the network lifetime and throughput by configuring beamforming nodes during the CB process. According to (14), the survival time of node i can be expressed as $T_i = 1/W_i$. We sort the survival times in ascending order as $\langle T_{(1)}, T_{(2)}, \dots, T_{(n)} \rangle$, and define network lifetime as the time when the number of nodes that have run out of energy exceeds the proportion p of the total network nodes. The network lifetime should be maximized, which can be expressed as follows:

$$f_1(\mathbb{I}) = T_{(\lceil p(n-1) \rceil + 1)}, \quad (20)$$

where $\mathbb{I} = \{I_{t,k} | 0 < t \leq T_{(\lceil p(n-1) \rceil + 1)}, k \in \mathcal{N}_t\}$ denotes excitation current weight sequence during the network lifetime.

Accordingly, let \bar{C}_{sink} be the average fused data packet size at the sink node, the network total throughput to the remote BS can be expressed as follows:

$$f_2(\mathbb{I}) = \bar{C}_{sink} T_{(\lceil p(n-1) \rceil + 1)}. \quad (21)$$

As can be seen, the two objectives are controlled by the same decision variable \mathbb{I} . The multi-objective-problem based on the aforementioned two objectives is formulated as follows:

$$\max_{\mathbb{I}} F = (f_1, f_2), \quad (22a)$$

$$\text{s.t. } 0 \leq I_{t,k} \leq 1, t \leq f_1 \quad \forall k \in \mathcal{N}, \quad (22b)$$

$$x_{ji} \in \{0, 1, 2\}, \quad \forall i, j \in \mathcal{N}, \quad (22c)$$

$$0 \leq \alpha_{i,j} \leq 1, \quad \forall i, j \in \mathcal{N}, \quad (22d)$$

$$d_{ij} \leq d_{max}, \quad \forall x_{ji} \in \{0, 1, 2\}, i, j \in \mathcal{N}, \quad (22e)$$

$$0 < p \leq 1. \quad (22f)$$

Based on the aforementioned analyses, we transform the problem of optimizing the decision variable \mathbb{I} into an MDP in the following.

C. MDP Formulation

Mathematically, an MDP can be denoted as a tuple $(\mathcal{S}, \mathcal{A}, \mathcal{P}, \mathcal{R}, \gamma)$, in which \mathcal{S} , \mathcal{A} , \mathcal{P} , \mathcal{R} , and γ denote the state set, action set, state transition probability, reward function and

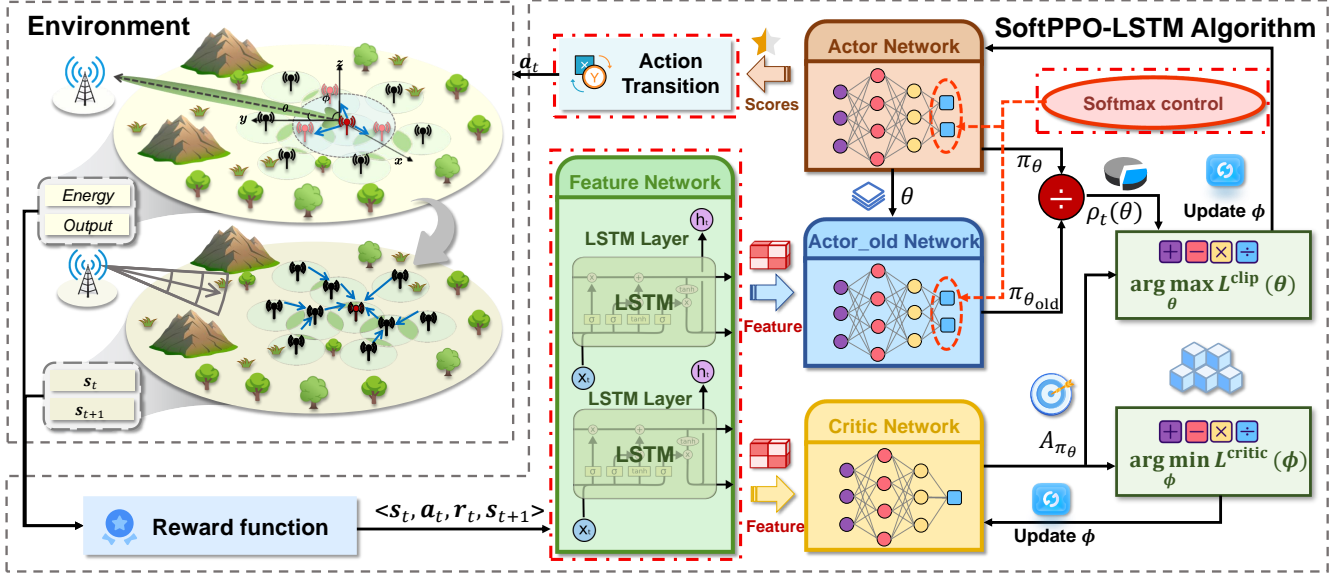


Fig. 5. Framework of SoftPPO-LSTM.

discount factor, respectively. Here, we detail the design of state space, action space, and reward in our model.

1) *State Space*: The state space includes residual energy and distance to the sink node, as these factors directly influence action decisions, further affecting the lifespan of the nodes, and the energy cost of the CB process. Moreover, the location information of the node is included in the state space, as nodes in different locations have varying degrees of location advantage. As such, the state s_t is as follows:

$$s_t = \{e_i(t), d_{i,s}(t) | i \in \mathcal{N}\}, \quad (23)$$

where $e_i(t)$ denotes the residual energy of node i , and $d_{i,s}(t)$ is the distance between node i and the sink node. These values can be derived or computed from the upstream packets of the nodes.

2) *Action Space*: After obtaining the state, the sink agent selects beamforming nodes. To ensure the received signal power at the remote BS is above the threshold for stable communication, the total power of beamforming nodes must be sufficient. Assuming all nodes participating in CB use rated power and perform perfect beamforming, only the selection of IoT nodes needs to be optimized. With the discrete action space, each node can be selected or unselected, resulting in an enormous action space size of 2^N . In this case, DRL methods face challenges in solving the problem, particularly when the number of IoT nodes N is large. Therefore, we convert the subset selection action into an N -dimensional continuous scoring vector for each node, substantially simplifying the problem-solving process. As such, the action of the sink agent a_t is as follows:

$$a_t = \{v_i(t) | i \in \mathcal{N}\}, \quad (24)$$

where $0 \leq v_i(t) \leq 1$ is the score of node i for acting as a beamforming node. In this case, the subset selection solution

is generated from a_t by sampling from the N -dimensional score vector, and the sampling satisfies the constraint (22b).

3) *Reward Function*: To extend the network lifetime and increase total throughput, the reward function considers the network energy consumption and the throughput delivered to the remote BS in each round, which is given as follows:

$$r_t = \zeta_1 C_t - \zeta_2 \sum_{i=1}^N (e_i(t) - e_i(t+1)), \quad (25)$$

where C_t is the throughput of the t th round, and $e_i(t)$ denotes the residual energy of node i in the t th round. The parameters ζ_1 and ζ_2 are the weights assigned to the throughput and the energy cost, respectively.

As can be seen, the MDP captures the essential aspects of the considered system by incorporating a comprehensive state space, a practical action space, and a carefully designed reward function. Note that the OMRP will influence the new state of the next round. This enables the DRL agent, which operates at the sink node, to adapt to the OMRP during training and improve the selection of decision variables \mathbb{I} . In the following, we will introduce the *SoftPPO-LSTM Algorithm*, which is tailored to leverage this MDP framework for enhanced network lifetime and throughput.

D. SoftPPO-LSTM Algorithm

In this subsection, we adopt PPO as the solving framework and present an enhanced version of the PPO algorithm, namely, SoftPPO-LSTM. SoftPPO-LSTM integrates two key features which are softmax control and LSTM layers to simplify the solution space and facilitate continuous and stable learning over long rounds.

1) *PPO Algorithm*: PPO is a state-of-the-art reinforcement learning algorithm based on policy. The objective of PPO is to

improve the policy parameters for achieving high state values, which is expressed as follows:

$$\max_{\theta} J(\theta) = \mathbb{E}_{\pi_{\theta}} \left[\sum_{t=1}^T \gamma^t r_t \right]. \quad (26)$$

Moreover, PPO enforces a clip on the ratio of the new policy probability to the old policy probability, thereby ensuring that policy updates are within a safe and bounded range. To this end, PPO improves the policy using a surrogate objective that constrains policy updates. Let $A_{\pi_{\theta}}$ be the advantage function, then the constraint is expressed as follows:

$$L^{clip}(\theta) = \mathbb{E}_t [\min(\rho_t(\theta) A_{\pi_{\theta}}(s_t, a_t), \rho_t^{clip}(\theta) A_{\pi_{\theta}}(s_t, a_t))], \quad (27)$$

where θ and $\rho_t(\theta)$ are the policy parameters and the ratio of new and old policy probabilities, respectively. Moreover, $\rho_t^{clip}(\theta) = clip(\rho_t(\theta), 1 - \epsilon, 1 + \epsilon)$ is a clipped value of $\rho_t(\theta)$, where ϵ is a hyperparameter that controls the size of the policy update. As such, PPO combines this surrogate objective with multiple epochs of data to iteratively update the policy while avoiding large policy deviations, resulting in stable learning.

However, in solving the considered MDP, one episode contains hundreds of timesteps, which lead to credit assignment issues [35]. At the same time, the packet routing in the environment is heuristic, and the long-term adaptability of the agent to the routing strategy is also a challenge. Furthermore, our system contains hundreds of IoT nodes, leading to a vast state and action space within the MDP framework. In particular, it is challenging for the PPO agent to produce continuous action space variables with hundreds of dimensions during hundreds of timesteps. In this case, we improve the PPO algorithm to make it suitable for our MDP in the following.

2) *Softmax Control-based Enhancement*: Softmax operations excel in handling classification selections and reducing the volatility of neuron signals, making them well-suited for our optimization problem. Therefore, we introduce softmax control to enhance the learning mechanism for our large-scale discrete action spaces. The softmax function is defined as follows:

$$\text{Softmax}(x) = \frac{e^{x_i}}{\sum_{i=1}^N e^{x_i}}. \quad (28)$$

By converting the outputs of the actor network into a probability distribution, softmax not only facilitates a nuanced understanding of the relative importance of each action but also guides the training process toward a more systematic exploration of these actions. Moreover, it also smooths gradients during backpropagation, ensuring stable policy updates and gradual model convergence, even in scenarios with sharp gradients.

3) *LSTM-based Network Structure*: Due to the complexity of time-series data in our problem, traditional models often struggle with managing long sequences of decisions and adapting to partially observable environments. Therefore, we introduce LSTM layers into the feature network of our SoftPPO-LSTM algorithm to enhance the temporal processing and inference capabilities. On the one hand, LSTMs excel in guiding training over long episodes with many timesteps, especially in our role allocation environments that unfold over extended periods.

Specifically, the LSTM unit consists of a cell, an input gate, an output gate, and a forget gate. The cell remembers values over arbitrary time intervals, while the gates regulate the flow of information into and out of the cell. This structure enables the LSTM to manage temporal dependencies by selectively filtering information at each time step. The operations of an LSTM cell at time step t can be described as follows:

$$f_t = \sigma(W_f \cdot [h_{t-1}, x_t] + b_f), \quad (29)$$

$$i_t = \sigma(W_i \cdot [h_{t-1}, x_t] + b_i), \quad (30)$$

$$\tilde{C}_t = \tanh(W_C \cdot [h_{t-1}, x_t] + b_C), \quad (31)$$

$$C_t = f_t * C_{t-1} + i_t * \tilde{C}_t, \quad (32)$$

$$o_t = \sigma(W_o \cdot [h_{t-1}, x_t] + b_o), \quad (33)$$

$$h_t = o_t * \tanh(C_t) \quad (34)$$

where σ denotes the sigmoid function, and $*$ denotes an element-wise multiplication. The variables f_t , i_t , and o_t are the forget, input, and output gates, respectively. The variables \tilde{C}_t , C_t , and h_t are the candidate cell state, the cell state, and the hidden state, respectively. On the other hand, LSTMs significantly enhance the ability to operate in environments characterized by partial observability. In our scenario, the environment first executes a heuristic-based routing policy to determine the current state, which is then provided as an observation to the DRL agent. The ability of LSTM to infer hidden states from sequences of partial observations fits well with this heuristic routing method, as it enables the DRL model to capture underlying patterns and dynamics and helps the agent better predict future states and make informed decisions. Consequently, this approach not only strengthens the strategic depth of the agent but also improves adaptability and overall performance in dynamically changing and partially observable environments.

4) *Main Steps of SoftPPO-LSTM algorithm for the CB Process*: As shown in Fig. 5, SoftPPO-LSTM employs two neural networks, *i.e.*, an actor neural network which is responsible for policy learning and a critic neural network that estimates the state value function and the advantage function. To ensure stable policy updates, SoftPPO-LSTM maintains an actor old network with identical parameters to calculate the clipping ratio. The current state s_t is fed into the feature network to produce features, which are then input into the actor network and critic network to generate the action a_t and the critic value, respectively. Following the execution of this action, the environment generates the corresponding reward r_t and the next state s_{t+1} . This process forms a fundamental transition within the framework of reinforcement learning.

The main steps of the proposed CB policy based on the SoftPPO-LSTM algorithm are shown in Algorithm 3. Specifically, the algorithm begins by initializing the neural network parameters. Then, SoftPPO-LSTM proceeds to execute episodes of interactions with the environment. Within each episode, the the environment and state are reset. For each time slot, the algorithm generates actions, interacts with the environment, and receives the reward and new state observations. Moreover, the algorithm periodically updates the actor and critic neural network parameters. This process repeats

until all specified episodes are completed, and the algorithm continuously refines its policy for reinforcement learning tasks.

4) *Complexity Analysis of SoftPPO-LSTM*: The computational and space complexity of SoftPPO-LSTM during training and execution phases are analyzed.

The computational complexity of SoftPPO-LSTM during the training phase is $\mathcal{O}((1+2MT)(|\theta_{Q_{new}}|+|\theta_c|+|\theta_f|)+(1+2MT/d)|\theta_{Q_{old}}|+NMT(V+2))$, which can be summarized as follows:

- *Network Initialization*: This phase involves the initialization of network parameters. Specifically, the computational complexity is expressed as $\mathcal{O}(|\theta_{Q_{new}}|+|\theta_c|+|\theta_f|+|\theta_{Q_{old}}|)$, where the $|\cdot|$ operation represents the number of parameters in the networks.
- *Action Transition*: This phase entails transforming actions according to the output scores of the actor network, and its complexity is $\mathcal{O}(NMT)$. Here, M denotes the number of training episodes, T is the number of steps per episode, and N is the number of IoT nodes.
- *Reward Calculation and State Transitions*: The computational complexity of reward calculation and state transitions is $\mathcal{O}(NMT(V+1))$, where V represents the complexity of interacting with the environment.
- *Network Update*: The updating phase is divided into three main parts that are frequent updates of the feature network and critic network, as well as less frequent updates of the actor network. Thus, the complexity of this phase is calculated as $\mathcal{O}(MT(2|\theta_{Q_{new}}|)+MT(2|\theta_c|)+MT(2|\theta_f|)+MT/d(2|\theta_{Q_{old}}|))$, where d is the updating interval of the old actor network.

Besides, the space complexity of SoftPPO-LSTM during the training phase is $\mathcal{O}(|\theta_{Q_{new}}|+|\theta_{Q_{old}}|+|\theta_f|+|\theta_c|+2|s|+|a|)$, where $|s|$ and $|a|$ denote the dimensions of the state and action spaces, respectively.

During the execution phase, the computational complexity of SoftPPO-LSTM is $\mathcal{O}(MT(|\theta_{Q_{old}}|+|\theta_f|)+NMT)$, which can be contributed by action selection and transition according to the current state using the feature and actor network. Moreover, the space complexity during the execution phase is $\mathcal{O}(|\theta_{Q_{old}}|+|\theta_f|+|s|)$ since the feature and actor network parameters need to be stored in memory for action selection.

VII. SIMULATION AND ANALYSIS

In this section, we present the simulation results and analyses for our IoT communication system, focusing on both routing methods and CB methods. We first introduce the simulation setting and benchmarks, and then provide the simulation results and analyses of the OMRP-based routing method and SoftPPO-LSTM-based CB method.

A. Simulation Setups

1) *Simulation Platform*: Our experiments are conducted using a computing setup that includes an NVIDIA GeForce RTX 4090 GPU with 24 GB of memory and a 13th Gen Intel(R) Core(TM) i9-13900K 32-core processor with 128 GB of RAM. The operating system on the workstation is Ubuntu

Algorithm 3: CB Policy based on SoftPPO-LSTM

```

1 Initialize actor network  $Q_{new}$  with parameters  $\theta_{Q_{new}}$ ,
  and then copy it to  $Q_{old}$ ;
2 Initialize the feature network denoted as  $\varepsilon_f$  with
  parameter  $\theta_f$ , and the critic network denoted as  $\varepsilon_c$ 
  with  $\theta_c$ ;
3  $step \leftarrow 0$ ;
4 for training episode = 1 to  $M$  do
5   Reset the environment and execute Algorithms. 1
     and 2 to get the initial state  $s_0$ ;
6   for round  $t = 1$  to  $T$  do
7     Select action  $\mathbf{a}_t = \{v_i(t) | i \in \mathcal{N}\}$ 
8     Transform  $\mathbf{a}_t$  into a node selection set by
       softmax and action sampling;
9     Execute CB strategy in the environment and
       generate the reward  $r_t$  by using Eq. (25);
10    Execute routing Algorithm. 1 and 2 to generate
      the the next state  $s_{t+1}$ ;
11    Update the critic network parameters  $\theta_c$ ;
12    Update the feature network parameters  $\theta_f$ ;
13    Update the new actor network parameters
       $\theta_{Q_{new}}$ ;
14    if  $step \bmod d$  then
15      Update the old actor network parameters
         $\theta_{Q_{old}}$  according to Eq. (27);
16    end
17     $step \leftarrow step + 1$ 
18  end
19 end

```

22.04.3 LTS. For our deep learning computations, we use PyTorch 2.0.1, along with CUDA 11.8.

2) *Environmental Details*: This study considers an IoT network consisting of 400 homogeneous IoT nodes, each equipped with a transmit power of 0.1 W. The IoT nodes are randomly deployed in a 200 m \times 200 m square region, with the remote BS located 1000 m outside the region at coordinates (100 m, 1200 m). Each IoT node operates at a bandwidth of 100 kHz, and the background noise level is set at -174 dBm/Hz. To ensure a balance between energy consumption for routing and CB processes while maintaining the quality of uplink communication, the minimum received power at the remote BS is set to -52 dBm [17].

In our scenario, since considerations of radiation interference and sidelobe levels are not necessary for the scenario, the excitation current weight for the nodes participating in CB is set to the maximum value of 1. Based on the above configurations, Eq. (4) shows that the involvement of 10 nodes in CB are sufficient to maintain normal communication quality, achieving a signal-to-noise ratio of approximately 24 dB. In addition, we consider the energy dissipation of the CB process as zero and the initial energy of each node E_0 as 4.0 J for the comparative analysis of the routing policies. Furthermore, the routing policy of the environment in the simulation of CB policies is configured to the proposed OMRP. Since synchronization and transmission energy dissipation in

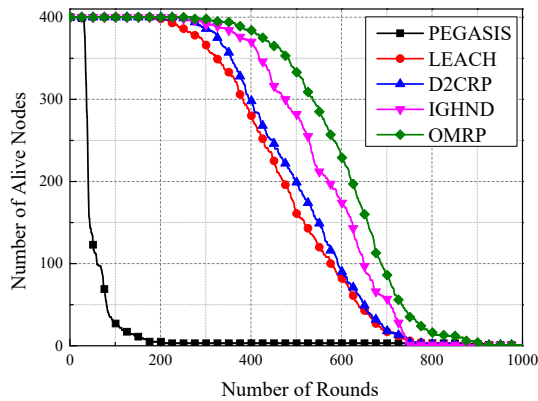


Fig. 6. Comparison of network lifetime.

TABLE II
SIMULATION PARAMETERS

Parameter	Value
Network size	200 m × 200 m
Position of the BS	(100 m, 1200 m)
Number of nodes: N	400
The monitor radius of IoT nodes	6.0 m
Initial energy of each node: E_0	4.0 J / 6.0 J
Altitudes of the IoT nodes: h_t	1.5 m
Altitudes of the BS: h_r	20 m
Energy dissipation-electronic circuit: E_{elec}	50 nJ/bit
Energy dissipation-free space amplifier: ϵ_{fs}	10 pJ/bit/m ²
Energy dissipation-multipath amplifier: ϵ_{mp}	0.0013 pJ/bit/m ⁴
Energy dissipation-data fusion: q_0	20 nJ/bit
Length of data packet	10000 bits
Length of control packet	200 bits

the CB process are considered, we set the initial energy of each node E_0 to 6.0 J. Table II provides other details about the radio model and the network.

B. Simulation and Analysis of OMRP

To demonstrate the superiority of our proposed OMRP, we compare OMRP with four well-known hierarchical routing protocols: PEGASIS [36], LEACH [17], D2CRP [19] and IGHND [37]. The experimental results are then analyzed with a focus on network lifetime, packet throughput, and the number of raw packets to the BS.

1) *Comparisons of Network Lifetime*: To demonstrate that the OMRP protocol can effectively slow down the death rate of nodes and extend the network lifetime, we show the relationship between the number of alive nodes and the number of running rounds of the five protocols in Fig. 6. Additionally, the simulation results of the round of first node death (FND), half node death (HND), and all node death (AND) are presented in Table III.

We can see from Fig. 6 that PEGASIS is the first protocol to experience node deaths, followed by LEACH, D2CRP, IGHND, and the proposed OMRP. As the rounds increase, the PEGASIS curve shows a steep decline, which can be attributed to the formation of long chains in PEGASIS, leading to higher energy dissipation during data fusion. As is shown in Table III, the overall network lifetime (measured by the round of AND)

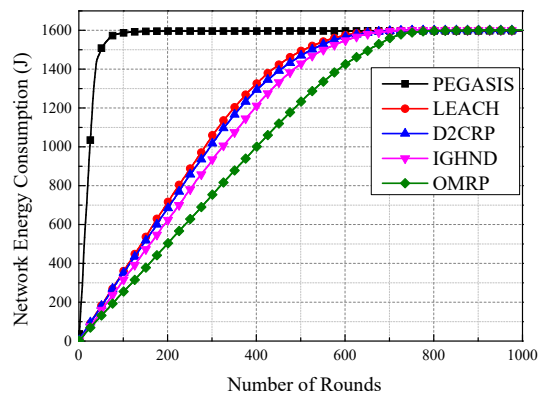


Fig. 7. Comparison of network energy consumption.

TABLE III
COMPARISON OF FND, HND, AND AND

Protocol	FND	HND	AND
PEGASIS	21	41	155
LEACH	187	473	733
D2CRP	236	499	743
IGHND	229	573	742
OMRP	271	624	870

under OMRP is approximately 19% longer than LEACH and 17% longer than both D2CRP and IGHND. It is clear that OMRP achieves the best performance in these three metrics due to its lower node death rate and longer network lifetime.

We attribute the slower node death rate of OMRP is mainly due to the introduction of the overlapping degree in the CH competition process. Nodes exhibiting higher overlapping degrees tend to be positioned closer to geographical center of the cluster, making their election as CHs conducive to reducing the transmission energy required by cluster members. By linking the likelihood of the election of a node as a CH to its overlapping degree, energy dissipation in the initial phases of the network is made more efficient.

TABLE IV
COMPARISONS OF FND-HND, HND-AND, AND 1-AND AVERAGE NETWORK ENERGY CONSUMPTION RATE.

Protocol	FND-HND	HND-AND	1-AND
PEGASIS	30.501 J/round	1.263 J/round	5.634 J/round
LEACH	2.762 J/round	0.547 J/round	1.707 J/round
D2CRP	2.509 J/round	0.539 J/round	1.561 J/round
IGHND	2.346 J/round	0.463 J/round	1.728 J/round
OMRP	2.215 J/round	0.571 J/round	1.540 J/round

2) *Comparisons of Network Energy Consumption*: The network energy consumption is used to measure the performance of the routing protocols. With no external energy supply, the protocol performs better if less energy is consumed in the network after the same rounds. The network energy consumption comparison of the five protocols is shown in Fig. 7 and Table IV. Specifically, the energy consumption rate of PEGASIS is very high during the period from the first node death to half of the dead node (FND-HND), which is almost six times

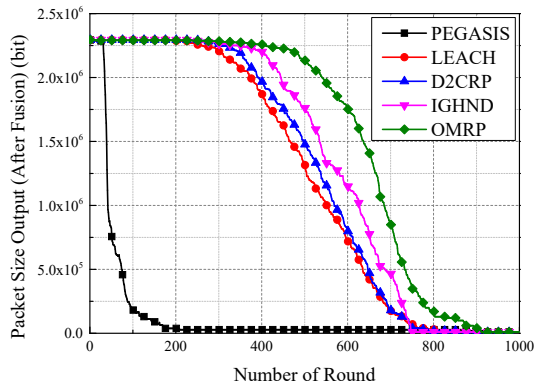


Fig. 8. Comparison of packet size output to BS.

the average energy consumption of the overall lifetime of the network (1-AND). In contrast, IGHND and OMRP display much smoother energy consumption rates. In particular, during the FND-HND phase, the energy consumption rate of OMRP is approximately 6%, 12%, 20%, and 92% lower than that of the IGHND, D2CRP, LEACH, and PEGASIS, respectively. Simulation results show that OMRP has the lowest energy consumption rate throughout the network lifetime.

Beyond CH election, the lower energy consumption of OMRP is attributed to the use of a multi-hop strategy and a communication sequence. Specifically, CHs adopt the available multi-hop mode to communicate with the sink node, establishing an optimized communication path within the cluster, which reduces transmission distance and energy consumption for inter-cluster communications. Additionally, based on the overlapping degree, the TDMA communication sequence within the cluster allows data with more redundancy to be compressed earlier, thereby reducing the energy consumption of CHs.

3) *Comparisons of Throughput to BS*: We evaluate network throughput by comparing the size of fused data packets and the count of raw packets sent to the BS across different routing protocols. The packet size reflects how well a protocol maintains data perception, while the raw packet count indicates its transmission efficiency. Figs. 8 and 9 show these comparisons, highlighting the performance of each protocol in terms of data perception and transmission efficiency, respectively.

TABLE V
COMPARISONS ON DATA PERCEPTION MAINTENANCE ABILITY.

Protocol	75%	50%	25%
PEGASIS	36	40	70
LEACH	427	524	627
D2CRP	453	554	641
IGHND	508	601	672
OMRP	608	674	723

Table V shows the maximum number of rounds various routing protocols can sustain at different throughput ratios. Specifically, OMRP shows an improvement in data perception maintenance ability by approximately 20%, 34%, and 42% at the 75% throughput ratio; 12%, 22%, and 29% at the 50% throughput ratio; and 8%, 13%, and 15% at the 25%

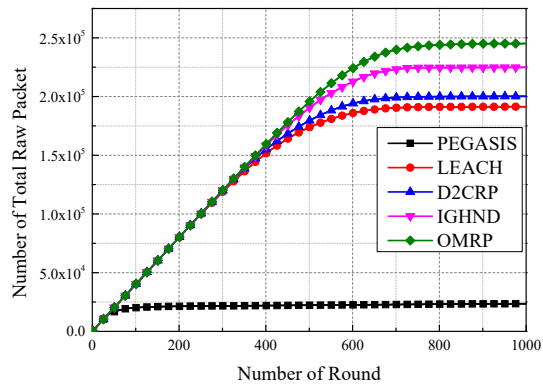


Fig. 9. Comparison of the number of raw packet to BS.

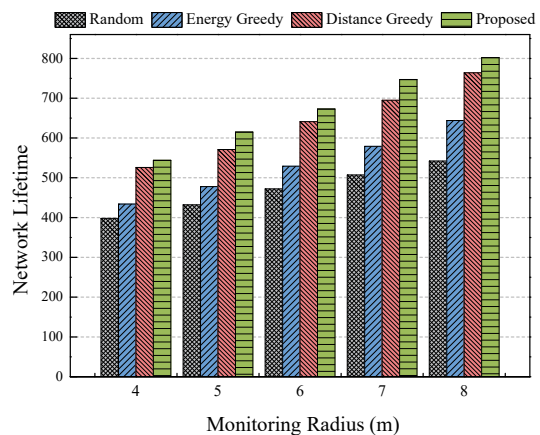


Fig. 10. Comparison of network lifetime under different monitoring radii.

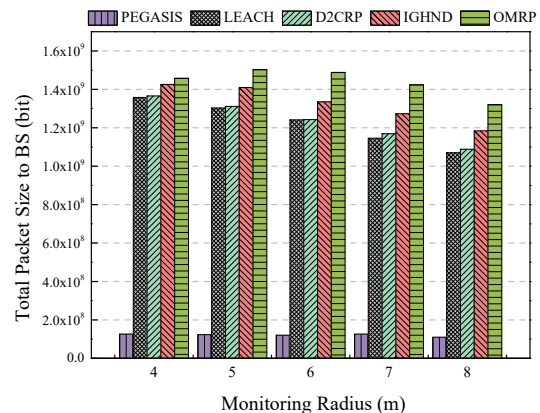


Fig. 11. Comparison of network throughput under different monitoring radii.

throughput ratio compared to IGHND, D2CRP, and LEACH, respectively. Furthermore, the total number of raw packets for OMRP increases by 9%, 22%, and 28% compared to IGHND, D2CRP, and LEACH, respectively.

4) *Analysis of the spatial correlation*: With the fixed node distribution and data packet size, the monitor radius r of the IoT nodes affects the degree of data spatial correlation. A larger r leads to more redundant data within the network. Figs. 10 and 11 show the network lifetime and total throughput

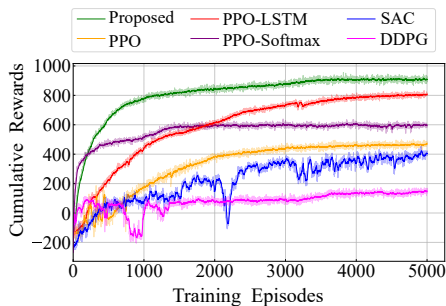


Fig. 12. Comparison of cumulative rewards.

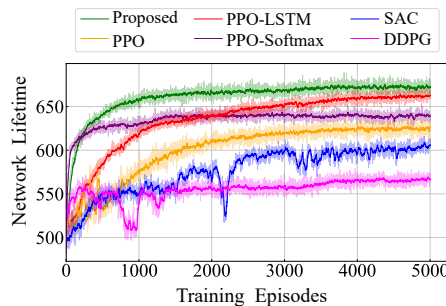


Fig. 13. Comparison of network life time.

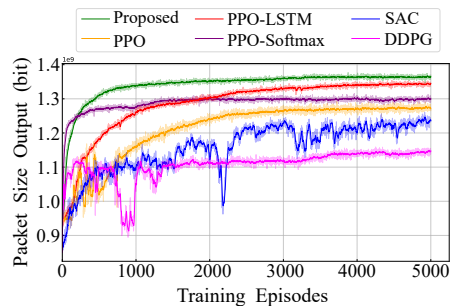


Fig. 14. Comparison of throughput to BS.

of the routing protocol under different values of r . It can be seen that OMRP performs best in network lifetime and total throughput in different scenarios.

C. Simulation of CB Method of SoftPPO-LSTM

For DRL comparative analysis, we employ benchmark methods including Deep Deterministic Policy Gradient (DDPG) [38], Soft Actor-Critic (SAC) [39], and Proximal Policy Optimization (PPO)[40] as reference models. We also compared the SoftPPO-LSTM-based CB method with the traditional greedy algorithm.

1) *Comparisons with DRL Policies*: Fig. 12 illustrates the cumulative rewards for each episode of SoftPPO-LSTM compared to other benchmark algorithms. Notably, the algorithms do not converge to the same solutions, which is due to the long episode lengths, the complexity of the MDP, and the high dimension of the action space, highlighting the challenge of the problem.

For the benchmark algorithms, DDPG employs Gaussian noise to diversify strategic actions but struggles to fully explore the high-dimensional action space. It quickly converges to the local optimal strategy and shows less stable learning of superior strategies. Although the SAC algorithm can identify relatively advantageous strategies, its learning trajectory exhibits significant fluctuations in our environment. Similarly, the learning trajectory of PPO exhibits fluctuations in the early training stages. However, PPO ultimately stands out for its robust performance in our environment with intricate action spaces.

Based on the strengths of PPO, the SoftPPO-LSTM algorithm further improves stability and performance by introducing softmax and LSTM techniques. Specifically, softmax greatly improved the stability of the agent in the early stages of training, demonstrating a fast and steady learning pace initially. The performance gains from LSTM are more pronounced in the middle and later stages of training. While the initial learning speed improvement from LSTM is not as impressive as that from softmax, its consistent and stable learning enables the agent to achieve better convergence strategies and higher rewards. The SoftPPO-LSTM algorithm integrates both softmax and LSTM enhancements, allowing the agent to develop a nuanced understanding of actions and a deep perception of the environment. As a result, it demonstrates the most stable learning ability and the highest reward score

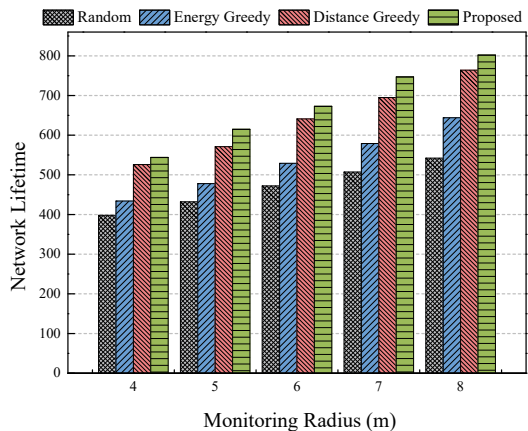


Fig. 15. Comparison of network lifetime under different monitoring radii.

in Fig. 12. Furthermore, as shown in Figs. 13 and 14, the trends of network lifetime and throughput are consistent with the cumulative rewards performance.

2) *Comparisons with Traditional Policies*: We evaluate three traditional strategies including random strategy, energy-based greedy strategy, and distance-based greedy strategy. The energy-based greedy strategy selects the nodes with the highest residual energy for CB, while the distance-based greedy strategy selects the nodes nearest to the sink node. In addition, Figs. 15 and 16 compare the network lifetime and throughput of these traditional strategies with SoftPPO-LSTM under different values of r . The simulation results show that SoftPPO-LSTM consistently achieves the highest throughput and the longest network lifetime.

Additionally, we evaluate the perception ability of SoftPPO-LSTM alongside these traditional strategies and analyze the performance. As is shown in Fig. 17, the random and energy-based greedy strategies exhibit a rapid decline in the early stages due to their failure to consider distance in broadcasting, leading to a large broadcast radius and high energy consumption. In contrast, the distance-based greedy strategy slows node death in the early stages but falls quickly in the later stages. We recorded the simulation process of the distance-based greedy strategy and found that the surviving nodes in the later stages are often found at the edge of the network, which increased the routing distance and accelerated node death. Although SoftPPO-LSTM does not outperform the distance-

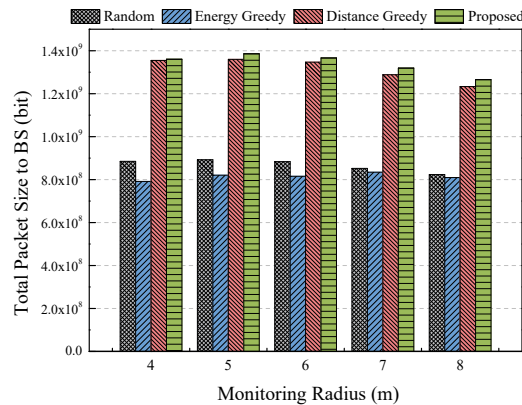


Fig. 16. Comparison of network throughput under different monitoring radii.

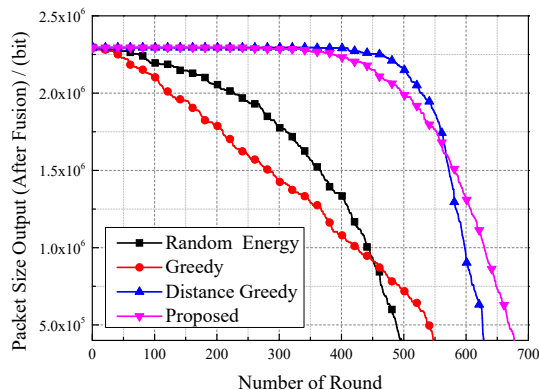


Fig. 17. Comparison of packet size output to BS in each round.

based greedy strategy initially, its comprehensive consideration of both locations and residual energy levels can ease the hot spot issue that the distance-based greedy strategy has. As a result, SoftPPO-LSTM maintains slower node death rates in the later stages, ultimately achieving the longest network lifetime and highest throughput.

VIII. CONCLUSION

In this article, we have studied a novel data-driven communication scheme for homogeneous IoT networks by integrating CB with routing protocols. Specifically, we have first utilized the OMRP to aggregate the network data at a specific node. Based on this aggregation, we have formulated a node selection problem for the CB stage aimed at optimizing uplink communication. Given the complexity of this problem, we have introduced the SoftPPO-LSTM algorithm, which intelligently selects CB nodes to enhance transmission efficiency. Simulation results indicate that the proposed OMRP demonstrated superior performance in extending network lifetime, minimizing energy consumption, and optimizing data throughput compared to existing protocols such as PEGASIS, LEACH, D2CRP, and IGHND. The introduction of the overlap degree in the CH election and the dynamic multi-hop strategies significantly contributed to these improvements. Moreover, the SoftPPO-LSTM-based CB policy employs the softmax control and LSTM layers to simplify the solution space and facilitate

stable learning over long rounds. These adjustments enable the IoT networks to reduce the energy consumption of the CB process while avoiding possible hot spot problems.

Future research will explore the adaptability of this mechanism in dynamic and heterogeneous network environments, including considerations of mobility and varying node densities. Further investigation will also focus on the potential of advanced machine learning algorithms to refine the CB strategy and routing protocols in real-time scenarios.

REFERENCES

- [1] F. Yang, Q. Sun, Z. Zhao, X. Wang, J. Xu, Y. Zheng, H. Zhang, and L. Wang, "Environment fusion routing protocol for wireless sensor networks," *IEEE Sensors J.*, 2023.
- [2] H. Qin, N. Li, T. Wang, G. Yang, and Y. Peng, "CDT: Cross-interface Data Transfer scheme for bandwidth-efficient LoRa communications in energy harvesting multi-hop wireless networks," *J. Netw. Comput. Appl.*, p. 103935, 2024.
- [3] L. Yang, B. Ma, L. Yuan, and B. Wu, "Effective application of IoT power electronics technology and power system optimization control," *Tsinghua Sci. Technol.*, vol. 29, no. 6, pp. 1763–1775, 2024.
- [4] S. Verma, Y. Kawamoto, Z. M. Fadlullah, H. Nishiyama, and N. Kato, "A survey on network methodologies for real-time analytics of massive IoT data and open research issues," *J Ambient Intell Humaniz Comput.*, vol. 19, no. 3, pp. 1457–1477, 2017.
- [5] S. R. Jan, R. Khan, F. Khan, M. A. Jan, M. D. Alshehri, V. Balasubramaniam, and P. S. Sehdev, "Marginal and average weight-enabled data aggregation mechanism for the resource-constrained networks," *Comput. Commun.*, vol. 174, pp. 101–108, 2021.
- [6] B. A. Begum and S. V. Nandury, "Data aggregation protocols for WSN and IoT applications—A comprehensive survey," *J King Saud Univ Comput Inf Sci.*, 2023.
- [7] P. Rawat and S. Chauhan, "A survey on clustering protocols in wireless sensor network: Taxonomy, comparison, and future scope," *J Ambient Intell Humaniz Comput.*, vol. 14, no. 3, pp. 1543–1589, 2023.
- [8] H. Ochiai, P. Mitran, H. V. Poor, and V. Tarokh, "Collaborative beamforming for distributed wireless ad hoc sensor networks," *IEEE Trans. Signal Process.*, vol. 53, no. 11, pp. 4110–4124, 2005.
- [9] G. Sun, X. Zhao, G. Shen, Y. Liu, A. Wang, S. Jayaprakasam, Y. Zhang, and V. C. Leung, "Improving performance of distributed collaborative beamforming in mobile wireless sensor networks: A multiobjective optimization method," *IEEE Internet Things J.*, vol. 7, no. 8, pp. 6787–6801, 2020.
- [10] O. B. Smida and S. Affes, "Dual-hop robust distributed collaborative beamforming over nominally rectangular wsns in slightly to moderately scattered environments," in *Proc. IWCMC*, 2023, pp. 1015–1021.
- [11] H. Jung and I.-H. Lee, "Secrecy performance analysis of analog cooperative beamforming in three-dimensional gaussian distributed wireless sensor networks," *IEEE Trans. Wireless Commun.*, vol. 18, no. 3, pp. 1860–1873, 2019.
- [12] A. Wang, Y. Wang, G. Sun, J. Li, S. Liang, and Y. Liu, "Uplink data transmission based on collaborative beamforming in UAV-assisted MWSNs," in *Proc. IEEE GLOBECOM*, 2021, pp. 1–6.
- [13] X. Bao, H. Liang, Y. Liu, and F. Zhang, "A stochastic game approach for collaborative beamforming in SDN-based energy harvesting wireless sensor networks," *IEEE Internet Things J.*, vol. 6, no. 6, pp. 9583–9595, 2019.
- [14] G. Sun, Y. Liu, Z. Chen, A. Wang, Y. Zhang, D. Tian, and V. C. Leung, "Energy efficient collaborative beamforming for reducing sidelobe in wireless sensor networks," *IEEE Trans. Mob. Comput.*, vol. 20, no. 3, pp. 965–982, 2019.
- [15] T. Liu, X. Qu, W. Tan, R. Wen, and L. Yang, "Energy-efficient joint collaborative and passive beamforming for intelligent-reflecting-surface-assisted wireless sensor networks," *IEEE Internet Things J.*, vol. 10, no. 19, pp. 17 193–17 205, 2023.
- [16] M. Z. Hasan, S. A. Alabady, and M. F. M. Salleh, "Power control for collaborative sensors in internet of things environments using k-means approach," in *Proc. ACN*, 2023, pp. 209–224.
- [17] W. B. Heinzelman, "Application-specific protocol architectures for wireless networks," Ph.D. dissertation, Massachusetts Institute of Technology, 2000.

- [18] T. M. Behera, S. K. Mohapatra, U. C. Samal, M. S. Khan, M. Daneshmand, and A. H. Gandomi, "Residual energy-based cluster-head selection in WSNs for IoT application," *IEEE Internet Things J.*, vol. 6, no. 3, pp. 5132–5139, 2019.
- [19] C. Chen, L.-C. Wang, and C.-M. Yu, "D2CRP: A novel distributed 2-hop cluster routing protocol for wireless sensor networks," *IEEE Internet Things J.*, vol. 9, no. 20, pp. 19 575–19 588, 2022.
- [20] D. Lin, Z. Lin, L. Kong, and Y. L. Guan, "CMSTR: A constrained minimum spanning tree based routing protocol for wireless sensor networks," *Ad Hoc Netw.*, vol. 146, p. 103160, 2023.
- [21] B. Wang, H. B. Lim, and D. Ma, "A coverage-aware clustering protocol for wireless sensor networks," *Comput. Netw.*, vol. 56, no. 5, pp. 1599–1611, 2012.
- [22] Y. Tao, Y. Zhang, and Y. Ji, "Flow-balanced routing for multi-hop clustered wireless sensor networks," *Ad hoc networks*, vol. 11, no. 1, pp. 541–554, 2013.
- [23] X. Song, T. Wen, W. Sun, D. Zhang, Q. Guo, and Q. Zhang, "A coverage-aware unequal clustering protocol with load separation for ambient assisted living based on wireless sensor networks," *China Commun.*, vol. 13, no. 5, pp. 47–55, 2016.
- [24] D. Kavitha and A. Chinnasamy, "Ai integration in data driven decision making for resource management in Internet of Things(IoT): A survey," in *Proc. IEMECON*, 2021, pp. 1–5.
- [25] I. Snigdh, S. S. Surani, and N. K. Sahu, "Energy conservation in query driven wireless sensor networks," *Microsyst. Technol.*, vol. 27, no. 3, pp. 843–851, 2021.
- [26] P. Biswas and T. Samanta, "True event-driven and fault-tolerant routing in wireless sensor network," *Wireless Pers. Commun.*, vol. 112, no. 1, pp. 439–461, 2020.
- [27] V. Saeidi, B. Pradhan, M. O. Idrees, and Z. Abd Latif, "Fusion of airborne LiDAR with multispectral SPOT 5 image for enhancement of feature extraction using Dempster–Shafer theory," *IEEE Trans. Geosci. Remote Sens.*, vol. 52, no. 10, pp. 6017–6025, 2014.
- [28] J. Wang, O. T. Tawose, L. Jiang, and D. Zhao, "A new data fusion algorithm for wireless sensor networks inspired by hesitant fuzzy entropy," *Sensors-basel.*, vol. 19, no. 4, p. 784, 2019.
- [29] X. Yu, W. Peng, K. Zhang, Z. Zhou, and Y. Liu, "Data fusion algorithm of wireless sensor network based on clustering and fuzzy logic," *Telecommun. Syst.*, pp. 1–10, 2024.
- [30] B. B. Haro, S. Zazo, and D. P. Palomar, "Energy efficient collaborative beamforming in wireless sensor networks," *IEEE Trans. Signal Process.*, vol. 62, no. 2, pp. 496–510, 2013.
- [31] S. Jayaprakasam, S. K. A. Rahim, and C. Y. Leow, "PSOGSA-Explore: A new hybrid metaheuristic approach for beampattern optimization in collaborative beamforming," *Appl. Soft Comput.*, vol. 30, pp. 229–237, 2015.
- [32] W. B. Heinzelman, A. P. Chandrakasan, and H. Balakrishnan, "An application-specific protocol architecture for wireless microsensor networks," *IEEE Trans Wirel Commun.*, vol. 1, no. 4, pp. 660–670, 2002.
- [33] C. Hua and T.-S. P. Yum, "Optimal routing and data aggregation for maximizing lifetime of wireless sensor networks," *IEEE ACM Trans. Netw.*, vol. 16, no. 4, pp. 892–903, 2008.
- [34] H. Luo, J. Luo, Y. Liu, and S. K. Das, "Adaptive data fusion for energy efficient routing in wireless sensor networks," *IEEE Trans. Comput.*, vol. 55, no. 10, pp. 1286–1299, 2006.
- [35] Q. Chen, Q. Zhang, and Y. Liu, "Balancing exploration and exploitation in episodic reinforcement learning," *Expert Syst. Appl.*, vol. 231, p. 120801, 2023.
- [36] S. Lindsey and C. S. Raghavendra, "PEGASIS: Power-efficient gathering in sensor information systems," in *Proc. IEEE AeroConf*, vol. 3, 2002, pp. 3–3.
- [37] H. Farman, B. Jan, H. Javed, N. Ahmad, J. Iqbal, M. Arshad, and S. Ali, "Multi-criteria based zone head selection in internet of things based wireless sensor networks," *Future Gener. Comp. Sy.*, vol. 87, pp. 364–371, 2018.
- [38] T. P. Lillicrap, J. J. Hunt, A. Pritzel, N. Heess, T. Erez, Y. Tassa, D. Silver, and D. Wierstra, "Continuous control with deep reinforcement learning," *arXiv preprint arXiv:1509.02971*, 2015.
- [39] T. Haarnoja, A. Zhou, K. Hartikainen, G. Tucker, S. Ha, J. Tan, V. Kumar, H. Zhu, A. Gupta, P. Abbeel *et al.*, "Soft actor-critic algorithms and applications," *arXiv preprint arXiv:1812.05905*, 2018.
- [40] J. Schulman, F. Wolski, P. Dhariwal, A. Radford, and O. Klimov, "Proximal policy optimization algorithms," *arXiv preprint arXiv:1707.06347*, 2017.